pH in atomic scale simulations of electrochemical interfaces

Rossmeisl, Jan; Chan, Karen; Ahmed, Rizwan; Tripkovic, Vladimir; Björketun, Mårten E.

Published in:
Physical Chemistry Chemical Physics

Link to article, DOI:
10.1039/c3cp51083b

Publication date:
2013

Document Version
Publisher's PDF, also known as Version of record

PCCP

RSC Publishing

COMMUNICATION

pH in atomic scale simulations of electrochemical interfaces

Cite this: *Phys. Chem. Chem. Phys.*, 2013, **15**, 10321

Received 12th March 2013,
Accepted 9th May 2013

DOI: 10.1039/c3cp51083b

www.rsc.org/pccp

Jan Rossmeisl,*[a] Karen Chan,[ab] Rizwan Ahmed,[a] Vladimir Tripković[a] and Mårten E. Björketun[a]

Electrochemical reaction rates can strongly depend on pH, and there is increasing interest in electrocatalysis in alkaline solution. To date, no method has been devised to address pH in atomic scale simulations. We present a simple method to determine the atomic structure of the metal|solution interface at a given pH and electrode potential. Using Pt(111)|water as an example, we show the effect of pH on the interfacial structure, and discuss its impact on reaction energies and barriers. This method paves the way for *ab initio* studies of pH effects on the structure and electrocatalytic activity of electrochemical interfaces.

Electrocatalysis is a central part of research and development in energy conversion technologies. Recent improvements in computational power and theory have allowed for density functional theory (DFT) calculations on electrochemical systems, which have driven the development of new electrocatalysts.[1–3] Currently, there are two main types of *ab initio* studies on electrochemical systems. Catalyst screening/optimization studies focus on adsorption free energies of reaction intermediates. Water and electric fields are often omitted to reduce the computational resources,[4] and the effect of potential is added *a posteriori via* the computational hydrogen electrode.[5] Fundamental studies focus on setting up an explicit electrode potential and electric field at the interface, *via* water layers, excess free charge, counter-ions, and counter electrodes.[6–10]

No existing approach addresses the effect of pH on the interfacial structure. Electrochemical reaction rates can, however, be strongly affected by solution pH, and there is increasing interest in the development of efficient electrocatalysts for alkaline environments.[11–14] Consideration of pH is thus a crucial challenge in *ab initio* simulations.

In this communication, we present a novel generalization of the computational hydrogen electrode to explicitly capture the respective pH and potential effects on the interface structure and its corresponding free energy. Using simple thermodynamic arguments, the method determines ground state interface structures as a function of pH and potential. As an example, we apply the method to a set of Pt(111)|water structures and determine the corresponding Pourbaix diagram. This method opens up the possibility for theoretical studies of pH effects on the structure and electrocatalytic activity of electrochemical interfaces.

We first review the Born–Haber cycle for hydrogen oxidation, shown in Fig. 1, which gives the relation among the electrode potential U, pH, and electrochemical potential of protons and electrons, $\mu_{H^++e^-}$.[15] With the chemical potential of gas phase H_2 as the zero reference point, the free energy of the reaction is

$$\mu_{H^++e^-} = \Delta_d G + \Delta_i G - \Phi_{H^+} - \Phi_{e^-}, \quad (1)$$

where $\Delta_d G$ is the $1/2H_2$ dissociation energy, $\Delta_i G$ the H ionization energy, and Φ_{H^+} and Φ_{e^-} the respective work functions of H^+ in solution and e^- in metal, measured with respect to vacuum just outside the solution phase. The pH dependence on $\mu_{H^++e^-}$ arises from the proton free energy, *i.e.*

$$\Phi_{H^+} = \Phi^0_{H^+} + 2.3\,kT \cdot \mathrm{pH} \quad (2)$$

The standard hydrogen electrode (SHE) potential corresponds to electrochemical equilibrium, $\mu_{H^++e^-} = 0$, at pH = 0, and the corresponding work function Φ_{e^-}(SHE) has the experimentally determined value of 4.44 eV.[15] The reversible hydrogen electrode (RHE) corresponds to $\mu_{H^++e^-} = 0$ at arbitrary pH.

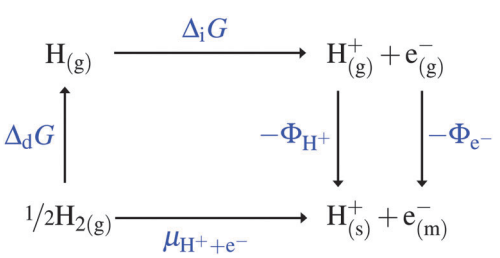

Fig. 1 The Born–Haber cycle for hydrogen oxidation.[15]

[a] *Center for Atomic-scale Materials Design, Department of Physics, Technical University of Denmark, DK-2800 Lyngby, Denmark. E-mail: jross@fysik.dtu.dk; Fax: +45 4593 2399; Tel: +45 4525 3166*
[b] *Department of Chemistry, Simon Fraser University, Burnaby, BC, Canada*

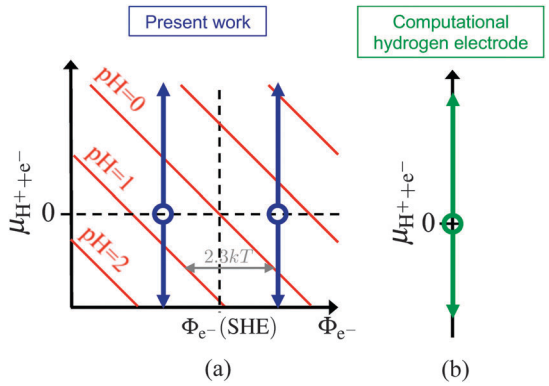

Fig. 2 (a) Eqn (3) mapped as red iso-pH lines on the (Φ_{e^-}, $\mu_{H^+ + e^-}$)-plane. Projections of G^{int} *vs.* $\mu_{H^+ + e^-}$ of the present work in blue arrows, where Φ_{e^-} is determined by the interfacial structure. (b) Projection of G^{int} *vs.* $\mu_{H^+ + e^-}$ of the computational hydrogen electrode in green arrows, where Φ_{e^-} is not considered.[5]

The electrochemical potential can be written simply in terms of Φ_{e^-}(SHE), pH, and Φ_{e^-},

$$\mu_{H^+ + e^-} = \Phi_{e^-}(\mathrm{SHE}) - 2.3\ kT \cdot \mathrm{pH} - \Phi_{e^-}. \quad (3)$$

The electrode potential U, which is determined by the interface dipoles in the computational model, is directly proportional to Φ_{e^-}.[15,16] Relative to, *e.g.*, the SHE reference electrode,

$$U_{\mathrm{SHE}} = \frac{\Phi_{e^-} - \Phi_{e^-}(\mathrm{SHE})}{e}. \quad (4)$$

Fig. 2(a) plots eqn (3) in red iso-pH lines on the (Φ_{e^-}, $\mu_{H^+ + e^-}$)-plane. The core of the method presented here is: for a given metal|solution structure, if Φ_{e^-} and $\mu_{H^+ + e^-}$ are known, the corresponding pH is determined *via* eqn (3).

We now describe an extrapolation scheme to determine the integral free energy, G^{int}, of interfacial structures on the (Φ_{e^-}, $\mu_{H^+ + e^-}$)-plane. For a given structure, Φ_{e^-} and the interface dipole are constant. The free energy per surface metal atom at electrochemical equilibrium, $\mu_{H^+ + e^-} = 0$, is

$$G^{\mathrm{int}}(\mu_{H^+ + e^-} = 0, \Phi_{e^-}) = \frac{G_{N,n} - G_{N,0}}{N} - \frac{1}{2}\frac{n}{N}G_{H_2}, \quad (5)$$

where n is the number of hydrogens (as $H^+ + e^-$, or as adsorbates, H_{ad}, OH_{ad}, and O_{ad}), N the number of surface metal atoms, $G_{N,n}$ the free energy of the metal|solution system of interest, $G_{N,0}$ the free energy of a reference system with no ions or adsorbates, and G_{H_2} the free energy of gas-phase H_2 under standard conditions. All G are straightforward to obtain *via* DFT and standard tables. If oxide species are present, n can be negative. Here, we consider equilibrium with the hydrogen reference electrode. We obtain the energy of this reference state with the computed energy of hydrogen gas. This approach allows us to avoid ill-defined simulations of protons in solution.

The corresponding pH of the given structure can be calculated from eqn (3). G^{int} for the interface at another pH, where $\mu_{H^+ + e^-} \neq 0$, is given by the linear extrapolation,

$$G^{\mathrm{int}}(\mu_{H^+ + e^-}, \Phi_{e^-}) = G^{\mathrm{int}}(\mu_{H^+ + e^-} = 0, \Phi_{e^-}) - \frac{n}{N}\mu_{H^+ + e^-}. \quad (6)$$

Fig. 2(a) illustrates, on the (Φ_{e^-}, $\mu_{H^+ + e^-}$)-plane, the extrapolation for two interface structures of different Φ_{e^-}, in blue arrows. We note that for a specific system, the extrapolation in eqn (6) is performed at constant Φ_{e^-}, *i.e.* the variations in $\mu_{H^+ + e^-}$ are due to changes in pH.

At any given Φ_{e^-} and pH, the relevant ground state structure corresponds to that with minimum G^{int}. To map ground state metal|solution interfacial structures at a range of Φ_{e^-} and $\mu_{H^+ + e^-}$ (or pH) a representative set of interfacial structures of varying charge density, adsorbate coverage, and water dipoles should be considered. Electric fields that are consistent with pH and potential are automatically set up.

Fig. 2 shows the distinction between the G^{int} extrapolations of the present work (a, blue arrows) and the computational hydrogen electrode (b, green arrows).[5] Computational hydrogen electrode calculations do not consider the work function Φ_{e^-}, and extrapolation of G^{int} to $\mu_{H^+ + e^-} \neq 0$ are all done along a single line. The effect of potential is only considered *a posteriori via* $\mu_{H^+ + e^-} = -eU_{RHE}$, not in the physical interface dipole. Effects of water structure and interface electric fields on G^{int} are therefore neglected. In the present analysis, we consider explicitly Φ_{e^-} as fixed by the interface dipole, and map G^{int} on the (Φ_{e^-}, $\mu_{H^+ + e^-}$)-plane at the given Φ_{e^-}. This approach thereby distinguishes contributions of potential and pH to $\mu_{H^+ + e^-}$. Water structures and electric fields that are consistent with the pH and potential are automatically included. We discuss below the implications of the current analysis on previous results.

The present analysis is general in that it places no restrictions on the atomic interface model considered. Nothing is preassumed about $G_{N,n}$ and $G_{N,0}$ in eqn (5) and (6), and any atomic scale simulation of the electrochemical interface must include this analysis in order to explicitly and correctly account for pH and potential. With interface and bulk protons at electrochemical equilibrium, μ_{H^+}(interface) = μ_{H^+}(bulk), we can consider interface models with a limited number of water layers, provided that they fully screen the interface electric fields.[7,17]

To illustrate the method, we apply it to a variety of Pt(111)|water structures and determine the corresponding Pourbaix diagram. We consider 1–2 layers of ice-like hexagonal water structures[7,16,18] of a range of dipole orientations, adsorbate coverages (H_{ad}-covered, bare Pt, a 1/2 dissociated water layer), and H^+ concentrations. All model systems were charge neutral, such that the positive charge of the protons was balanced by a negative surface charge on the metal. The total number of systems was limited to ~110. Ideally, many more structures should be calculated to sample the corresponding partition function. An extended set of potentially relevant structures could be generated by performing molecular dynamics simulations, starting from different low energy structures. This is however beyond the scope of the present study.

DFT calculations were carried out with the Dacapo or GPAW code, integrated with the Atomic Simulation Environment.[19–22] The RPBE functional was used for exchange and correlation.[23] The density cutoff for plane wave Dacapo calculations was 350 eV while the grid spacing for GPAW real-space calculations was 0.2 Å. A Fermi smearing of 0.1 eV was used and energies

were extrapolated to an electronic temperature of 0 K. All systems contained a periodic 3-layer Pt(111) slab and 1–2 water bilayers with at least 12 Å vacuum in the direction perpendicular to the surface. An optimized Pt lattice constant of 4.02 Å was used in all calculations. Unit cells of sizes (3 × 2), (3 × 3), (3 × 4), (3 × 6), and (6 × 4) were sampled with Monkhorst–Pack *k*-point grids (4 × 6), (4 × 4), (4 × 3), (4 × 2), and (2 × 3). In all cases, a dipole correction was applied.[24] The two bottom layers were constrained and all other atoms relaxed until the forces on them were less than 0.05 eV Å^{-1}. To obtain the free energies G, the zero point energies and entropies of protons and adsorbed hydrogens were taken from ref. 5 and 17. The reference energy structure corresponding to $G_{N,0}$ was a bare slab with water layer(s) of equal density of H-up and H-down waters. For each simulation, $G^{\mathrm{int}}(\mu_{\mathrm{H^+}+\mathrm{e^-}} = 0, \Phi_{\mathrm{e^-}})$ was calculated and $\Phi_{\mathrm{e^-}}$ was measured. $G^{\mathrm{int}}(\mu_{\mathrm{H^+}+\mathrm{e^-}}, \Phi_{\mathrm{e^-}})$ was then calculated according to eqn (6).

Fig. 3 shows G^{int} for three sample Pt(111)|water structures. G^{int} was linearly extrapolated at the three corresponding $\Phi_{\mathrm{e^-}}$ with eqn (6). Constant pH = 0, 7, 14 planes are mapped perpendicular to the ($\Phi_{\mathrm{e^-}}$, $\mu_{\mathrm{H^+}+\mathrm{e^-}}$)-plane (eqn (3)). Intersections of the 3 lines with the pH planes are highlighted with flat circles, marking the G^{int} of the 3 structures at those particular pH's.

Fig. 4(a) and (b) show the full set of considered water structures as projections of G^{int} onto the pH = 0 and pH = 14 planes, respectively. The SHE scale is shown along the bottom *x*-axis, and the RHE scale along the top *x*-axis. The legend shows the dipole orientation of the water structure, with H-up water indicated by ↑ and H-down by ↓. The H concentration, n/N, is indicated by the colorbar.

We obtain a simple Pt(111)|water Pourbaix diagram by interpolating the results for select proton/adsorbate coverages, n/N = −0.33, 0, 0.17, 1, and 1.17. For these coverages, we fit straight lines through the G^{int} *vs.* potential data at a range of pH (*cf.* Fig. 4),

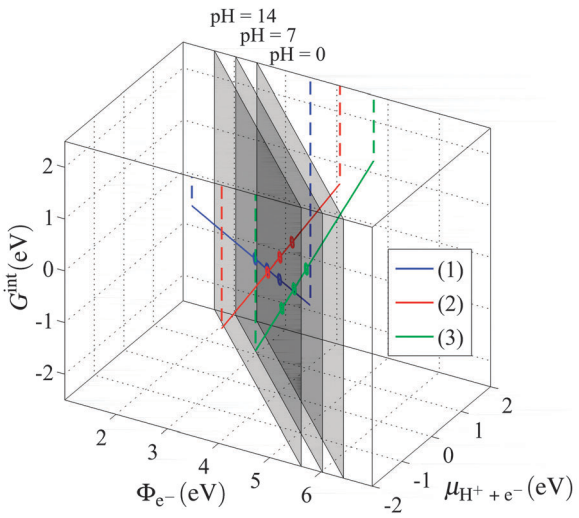

Fig. 3 Calculated G^{int} *vs.* $\Phi_{\mathrm{e^-}}$, $\mu_{\mathrm{H^+}+\mathrm{e^-}}$, for select Pt(111)|solution interfacial structures: (1) $\Phi_{\mathrm{e^-}}$ = 3.48 eV, n/N = 0.96, (2) $\Phi_{\mathrm{e^-}}$ = 4.06 eV, n/N = −0.22, (3) $\Phi_{\mathrm{e^-}}$ = 4.72 eV, n/N = −0.44. Dashed lines are shown as guides for the eye. Intersections of G^{int} with constant pH = 0, 7, 14 planes are marked with circles, indicating G^{int} at those particular pH.

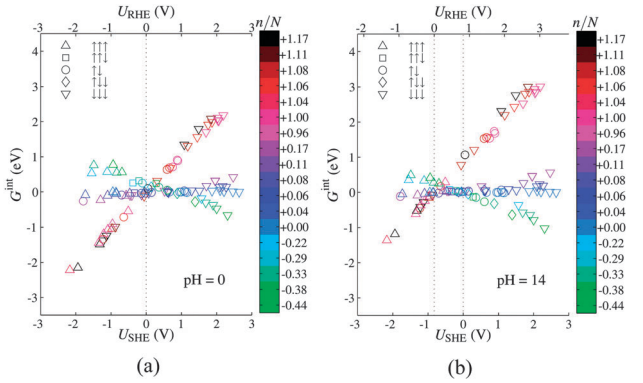

Fig. 4 Calculated G^{int} *vs.* *U* (*vs.* SHE and RHE) for all considered Pt(111)|solution interfacial structures, as projected onto (a) pH = 0 and (b) pH = 14 planes. The H concentration n/N is indicated by the colorbar, and the net dipole of the water by arrows.

and linearly interpolate both the G^{int} and dipole orientation. Then, at every *U* and pH, we pick out the most stable structure. The resultant Pourbaix diagram is shown in Fig. 5.

Consistent with experimental cyclic voltammograms and Pourbaix diagrams,[25,26] increasing *U* leads to a shift from a H_{ad} to OH_{ad} covered surface. The −0.059 eV/pH (−2.3 *kT*/pH) slope in the dotted lines dividing regions of different coverages show the expected U_{RHE} dependence of adsorbate coverage. Generally, as *U* increases and the surface changes from H_{ad} to OH_{ad} covered, water orientation tends to shift from H-up to H-down; this maximizes the hydrogen bonding between the adsorbates and water layer.[27,28] Water orients from H-down to H-up as pH increases, *i.e.* at low pH, H's tend to point toward the Pt surface. This trend is in agreement with that suggested by impedance spectroscopy.[29]

Calculated work functions are usually associated with a slight error, which introduces an uncertainty in the exact position of the systems relative to SHE and RHE. Correcting for this error

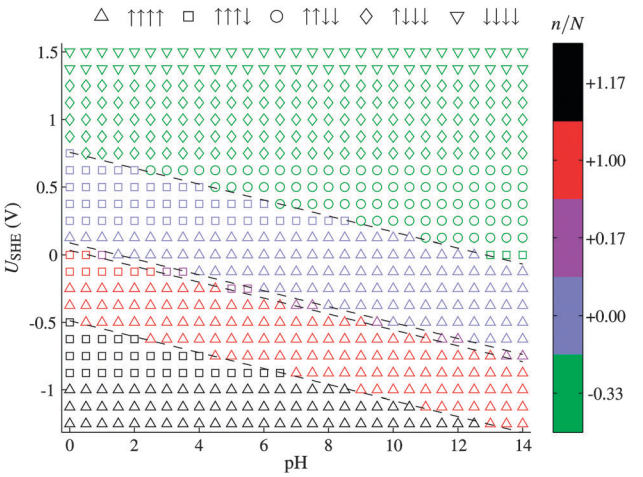

Fig. 5 Simulated Pourbaix diagram for Pt(111), showing the minimum energy structures as a function of pH and U_{SHE} for select excess H concentration n/N. Dotted lines dividing regions of different coverages have a −0.059 eV/pH slope, indicating the expected U_{RHE} dependence of adsorbate coverage.

would translate the systems along the different coverage lines in Fig. 4. This would change neither the preferred H coverage *vs.* SHE and RHE nor the observed trend in water orientation, but it could change the potential at which a certain water orientation starts to dominate. The precision of the method is strongly dependent on the accuracy of the DFT calculations. In any case, the trends allow us to at least distinguish between acidic, neutral, and alkaline conditions.

The Pt(111)|water example illustrates how pH and U affect the metal|solution interfacial structure. Essentially, the electrochemical potentials of both the protons and electrons are required to determine the ground state interfacial structure. Any U can be set up by a variety of adsorbate coverages, surface charge densities, and water dipole orientations. The electrochemical potential of the proton, determined by the pH, picks out the relevant minimum energy structure for a given U.

This new insight into the effect of pH on the interfacial structure does not necessarily invalidate previous computational hydrogen electrode studies, as long as the adsorbates of interest show negligible interactions with electric fields and water.[4,30] In this case, for a given adsorbate coverage, only differences in the water orientation contribute to the variation of G^{int} with Φ_{e^-}, and such contributions are negligible† compared to those of adsorbate binding energies. G^{int} then depends mainly on $\mu_{H^++e^-}$, not Φ_{e^-}, *i.e.* $G^{\mathrm{int}} \approx f(\mu_{H^++e^-}) = f(-eU_{\mathrm{RHE}})$. This leads to a simple U_{RHE} dependence of adsorbate coverage, as is the case for H_{ad} and OH_{ad} on Pt, considered above. G^{int} obtained *via* a computational hydrogen electrode and the present extrapolation (*cf.* Fig. 2) would then be very similar, even though water structures considered previously, if any, were likely not consistent with the ground state structures at the assumed pH and U. Where adsorbates are highly affected by field and/or water structure, *e.g.* adsorbates with substantial dipole moments,[30] and/or where adsorbate coverages do not show a simple U_{RHE} dependence,[31] the present analysis is required.

In reaction barrier studies, pH can have an important effect, as the barriers may be highly dependent on water structure. The ground state structures determined above could, for instance, explain the dramatically higher rates of hydrogen evolution on Pt in acidic solution than in basic ones.[11,12] At relevant electrode potentials and low pH, some hydrogens point toward the surface, which results in a very small barrier for proton transfer. At higher pH, all hydrogens point away from the surface, which gives rise to an extra barrier.

We have focussed on a simple model system of Pt(111)|water to illustrate the method. We expect more complex model systems with extended water layers, anions, and oxide species to further demonstrate the capabilities of the model, and detailed studies are in progress.

In summary, we have presented a simple scheme to determine the relevant interfacial structure at a given potential and pH, based on thermodynamic arguments. For any given interfacial structure containing any reaction intermediate of interest, the only required inputs to the analysis are the electron work function and the integral free energy, both easily determined using standard DFT. The method is in principle general, but as of today only rather idealized systems can be studied due to computational limitations. Applying the scheme to Pt(111)|water as an example, we show the pH to affect the adsorbate coverage and water orientation, which is expected to have an important impact on charge transfer reaction barriers. The method paves the way for *ab initio* studies of pH effects on the structure and electrocatalytic activity of electrochemical interfaces.

The CASE initiative is funded by the Danish Ministry of Science, Technology and Innovation. Support from DCSC is gratefully acknowledged. KC thanks NSERC for financial support.

† G^{int} ($\mu_{H^++e^-} = 0$) differences among neutral water layers of various dipoles are <0.1 eV.

References

1 J. Greeley, I. E. L. Stephens, A. S. Bondarenko, T. P. Johansson, H. A. Hansen, T. F. Jaramillo, J. Rossmeisl, I. Chorkendorff and J. K. Nørskov, *Nat. Chem.*, 2009, **1**, 552–556.
2 J. K. Nørskov, T. Bligaard, J. Rossmeisl and C. H. Christensen, *Nat. Chem.*, 2009, **1**, 37–46.
3 F. Calle-Vallejo and M. T. Koper, *Electrochim. Acta*, 2012, **84**, 3–11.
4 G. S. Karlberg, T. F. Jaramillo, E. Skúlason, J. Rossmeisl, T. Bligaard and J. K. Nørskov, *Phys. Rev. Lett.*, 2007, **99**, 126101.
5 J. K. Nørskov, J. Rossmeisl, A. Logadottir, L. Lindqvist, J. R. Kitchin, T. Bligaard and H. Jonsson, *J. Phys. Chem. B*, 2004, **108**, 17886–17892.
6 C. D. Taylor, S. A. Wasileski, J.-S. Filhol and M. Neurock, *Phys. Rev. B: Condens. Matter Mater. Phys.*, 2006, **73**, 165402.
7 J. Rossmeisl, E. Skúlason, M. E. Björketun, V. Tripkovic and J. K. Nørskov, *Chem. Phys. Lett.*, 2008, **466**, 68–71.
8 M. Otani and O. Sugino, *Phys. Rev. B: Condens. Matter Mater. Phys.*, 2006, **73**, 115407.
9 J. Cheng and M. Sprik, *Phys. Chem. Chem. Phys.*, 2012, **14**, 11245–11267.
10 S. Schnur and A. Groß, *Catal. Today*, 2011, **165**, 129–137.
11 N. M. Markovic, S. T. Sarraf, H. A. Gasteiger and P. N. Ross, *J. Chem. Soc., Faraday Trans.*, 1996, **92**, 3719–3725.
12 R. Subbaraman, D. Tripkovic, D. Strmcnik, K.-C. Chang, M. Uchimura, A. P. Paulikas, V. Stamenkovic and N. M. Markovic, *Science*, 2011, **334**, 1256–1260.
13 W. Sheng, H. A. Gasteiger and Y. Shao-Horn, *J. Electrochem. Soc.*, 2010, **157**, B1529–B1536.
14 R. Gisbert, G. García and M. T. M. Koper, *Electrochim. Acta*, 2011, **56**, 2443–2449.
15 S. Trasatti, *Pure Appl. Chem.*, 1986, **58**, 955–966.
16 V. Tripkovic, M. E. Björketun, E. Skúlason and J. Rossmeisl, *Phys. Rev. B: Condens. Matter Mater. Phys.*, 2011, **84**, 115452.
17 E. Skúlason, V. Tripkovic, M. E. Björketun, S. Gudmundsdóttir, G. S. Karlberg, J. Rossmeisl, T. Bligaard, H. Jónsson and J. K. Nørskov, *J. Phys. Chem. C*, 2010, **114**, 18182–18197.
18 H. Ogasawara, B. Brena, D. Nordlund, M. Nyberg, A. Pelmenschikov, L. G. M. Pettersson and A. Nilsson, *Phys. Rev. Lett.*, 2002, **89**, 276102.

19 *Dacapo pseudopotential code*, URL: https://wiki.fysik.dtu.dk/dacapo, Center for Atomic-scale Materials Design (CAMD), Technical University of Denmark, Lyngby, 2010.
20 J. J. Mortensen, L. B. Hansen and K. W. Jacobsen, *Phys. Rev. B: Condens. Matter Mater. Phys.*, 2005, **71**, 035109.
21 J. Enkovaara, C. Rostgaard, J. J. Mortensen, J. Chen, L. F. M. Dułak, J. Gavnholt, C. Glinsvad, V. Haikola, H. A. Hansen, H. H. Kristoffersen, M. Kuisma, A. H. Larsen, L. Lehtovaara, M. Ljungberg, O. Lopez-Acevedo, P. G. Moses, J. Ojanen, T. Olsen, V. Petzold, N. A. Romero, J. Stausholm-Møller, M. Strange, G. A. Tritsaris, M. Vanin, M. Walter, B. Hammer, H. Häkkinen, G. K. H. Madsen, R. M. Nieminen, J. K. Nørskov, M. Puska, T. T. Rantala, J. Schiøtz, K. S. Thygesen and K. W. Jacobsen, *J. Phys.: Condens. Matter*, 2010, **22**, 253202.
22 S. R. Bahn and K. W. Jacobsen, *Comput. Sci. Eng.*, 2002, **4**, 56–66.
23 B. Hammer, L. B. Hansen and J. K. Nørskov, *Phys. Rev. B: Condens. Matter Mater. Phys.*, 1999, **59**, 7413–7421.
24 L. Bengtsson, *Phys. Rev. B: Condens. Matter Mater. Phys.*, 1999, **59**, 12301.
25 M. Pourbaix, *Atlas of electrochemical equilibria in aqueous solutions*, Pergamon Press, 1966.
26 N. Garcia-Araez, V. Climent, E. Herrero, J. M. Feliu and J. Lipkowski, *Electrochim. Acta*, 2006, **51**, 3787–3793.
27 A. Peremans and A. Tadjeddine, *Phys. Rev. Lett.*, 1994, **73**, 3010–3013.
28 G. Jerkiewicz, G. Vatankhah, S.-i. Tanaka and J. Lessard, *Langmuir*, 2011, **27**, 4220–4226.
29 K. J. P. Schouten, M. J. T. C. van der Niet and M. T. M. Koper, *Phys. Chem. Chem. Phys.*, 2010, **12**, 15217–15224.
30 J. Rossmeisl, J. K. Nørskov, C. D. Taylor, M. J. Janik and M. Neurock, *J. Phys. Chem. B*, 2006, **110**, 21833–21839.
31 M. van der Niet, N. Garcia-Araez, J. Hernandez, J. M. Feliu and M. Koper, *Catal. Today*, 2013, **202**, 105–113.